High Pressure Research
Vol. 25, No. 2, June 2005, 107–118

Taylor & Francis
Taylor & Francis Group

A new belt-type apparatus for neutron-based rheological measurements at gigapascal pressures

DAVID P. DOBSON*†, JULIAN MECKLENBURGH‡, DARIO ALFE†§,
IAN G. WOOD† and MARK R. DAYMOND¶‖

†Department of Earth Sciences, University College London, Gower Street, London WC1E 6BT, UK
‡School of Earth, Atmospheric and Environmental Sciences, The University of Manchester, Oxford Road, Manchester, M13 9PL, UK
§Department of Physics and Astronomy, University College London, Gower Street, London, WC1E 6BT, UK
¶ISIS, Rutherford Appleton Laboratories, Chilton, Didcot, Oxfordshire, OX11 0QX, UK
‖Department of Mechanical and Materials Engineering, Queens University, Kingston, Ontario, Canada

(Received 15 March 2005; revised 14 April 2005; in final form 18 April 2005)

We have developed a new solid-media apparatus for performing rheological investigations at multi-gigapascal pressures. The pressure cell consists of a simple belt design and fits in a modified 250 tonne Paris–Edinburgh press. Elastic strains are measured by neutron diffraction, on the ENGIN-X experimental station at ISIS. Stresses are estimated from the measured strains in combination with published values of the elastic moduli. As an exemplair of the method, we present data from initial deformation experiments on pyrope garnet at 1.5 GPa and 873 K. Data collection times are as short as 60 min and the elastic strain resolution is better than 10^{-4}. We anticipate, however, that by interrupted testing, strain rates as low as 10^{-9}/s, or lower, will be measurable.

Keywords: High pressure; High temperature; Rheology; TOF neutron diffraction

1. Introduction

The knowledge of the rheology of the Earth's interior is of immense importance. The thermal and physical evolution of the Earth is controlled by convection in the solid silicate mantle, which extends from the brittle crust at ∼100 km depth to the liquid metal outer core at ∼2890 km. The strain rate in the mantle is very low, $\sim 10^{-14}$/s, but over the billions of years of geological history, the Earth's surface has been sculpted by the motion of the tectonic plates, which ride on the top of the mantle. The viscosity of the mantle is, however, among the least well constrained of all physical properties of the Earth. Traditional gas-media rheological equipment can only operate at relatively low pressures, up to 0.3 GPa (equivalent to ∼10 km depth). In contrast, solid-media multi-anvil and belt-type devices can achieve pressures in

*Corresponding author. Email: d.dobson@ucl.ac.uk

High Pressure Research
ISSN 0895-7959 print/ISSN 1477-2299 online © 2005 Taylor & Francis Group Ltd
http://www.tandf.co.uk/journals
DOI: 10.1080/08957950500143500

excess of 25 GPa, *i.e.* at pressures within the silicate perovskite stability field of the lower mantle.

Recently, there has been a considerable effort in developing rheological devices based around multi-anvil technologies. The high internal friction of solid pressure-media renders direct measurement of stress ineffectual. Rather, the new solid-media rheology devices use diffraction-based measurements of elastic strain as a proxy for stress. The new rheology devices therefore need high-penetration and high-flux radiation sources with a wavelength suitable for diffraction by atomic lattices. Weidner *et al.* [1] pioneered the use of synchrotron X-ray sources in measurements of differential stress as a development from the pseudo-hydrostatic multi-anvil equation of state studies of the 1980s and 1990s. As a further development, the d-DIA cell has the capability of independently moving two opposing anvils, varying the maximum and minimum stresses independently [2]. The precision of strain measurement in this type of X-ray study is, however, limited by the short wavelengths required for X-ray penetration of the pressure medium: diffraction patterns are measured at a 2θ angle of $\leq 6°$; the strain resolution is normally limited to $\sim 10^{-4}$, and measurements of low strain rates below 10^{-7}/s require very long experimental durations, not usually available at synchrotron sources (see [3] for a recent review).

We have developed a neutron-diffraction-based, solid-media device for measurements at low strain rates. Neutrons have a significantly higher penetration of most matters than X-rays. Consequently, a large range of wavelengths is available for high-pressure neutron diffraction experiments. With neutrons, time of flight (TOF) diffraction experiments may be performed at a fixed 2θ, so lattice planes at a single orientation are collected at a given detector, with the precision in measurement a function of the length of the neutron flight path. The ENGIN-X beamline at the CCLRC ISIS facility (Rutherford Appleton Laboratory, Chilton, UK) is optimised for strain-partitioning measurements [4]. Two detector banks collect diffracted neutrons at a 2θ of $+90°$ and $-90°$ with the diffraction vector in the horizontal plane (in practice the detector banks extend 15° above and below the horizontal). The total flight path is 51.5 m and lattice spacings can be measured to give tens of microstrain precision. If a sample is placed at the focus of the detectors, with the maximum and minimum resolved stresses oriented parallel to $\theta = \pm 45°$, each detector bank observes reflections from lattice planes oriented parallel to one of these principal stresses. Thus an axi-symmetric, solid-media device, with neutron access at $\pm 45°$ from the axis of compression, will provide the ideal geometry for TOF neutron diffraction-based rheological testing equipment, providing measurements of the elastic strain parallel and perpendicular to the axis of symmetry of the applied differential stress. Here we describe a belt-type device designed for this purpose and present preliminary results from strain relaxation tests on a natural pyrope garnet at 873 K. Silicate garnet is a substantial component of the lower crust and upper mantle and may play a key role in controlling the rheology of these regions [5]. In addition, the cubic symmetry of garnets provides an ideal initial test case for this new apparatus.

2. Cell design

Figure 1 shows a cross-section of the belt-type apparatus and press in the plane of diffraction. The press is a 250 tonne Paris–Edinburgh press [6], which was modified to take the belt-tooling by increasing the tie–rods from 159 to 299 mm in length. The cylindrical belt consists of a tungsten carbide core with a 10 mm diameter and 7 mm long sample cavity. The inner surface of the carbide core beyond the sample cavity is tapered at 47° from the axis of the cylinder, to a diameter of 39 mm. This core is compressed by a strip-wound stress ring, supplied by Strecon,

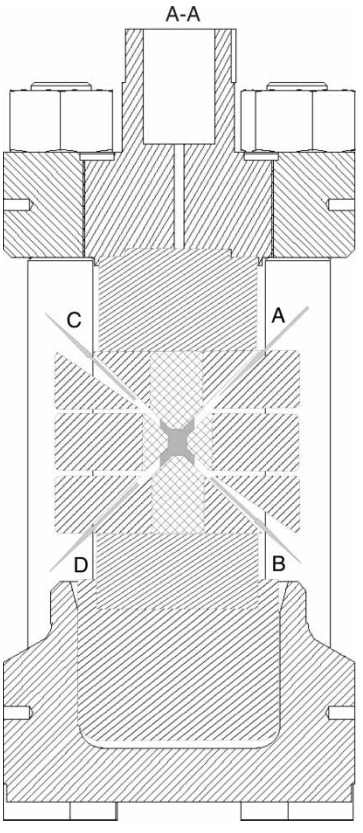

Figure 1. Cross-section of the belt-type press. Steel components are indicated with diagonal hatching, tungsten carbide is cross-hatched and the ceramic pressure medium and gaskets are represented in grey.

to an interference fit of 1.3%. This provides 1.5 GPa of compression to the outer surface of the carbide core. Tungsten carbide pistons comprise cones, truncated to 6 mm diameter, cut at 43° from the axis of the cylinder. The stress ring for the pistons is manufactured from solid high-tensile steel, with slots cut at 45° for neutron access, labelled A–D on the figure. The incident and transmitted beam slots (A and D) are 6 mm diameter parallel-sided cylinders, whereas the diffracted beam slots extend to $\pm 5°$ in 2θ and $\pm 12°$ in ϕ. This arrangement provides sufficient access for the diffracted beam without significantly affecting the structural integrity of the pistons. The tapers of the pistons and carbide core result in a 4° gasket taper, narrowing towards the sample. This taper enhances the pressure gradient along the gaskets, ensuring that they provide the maximum support to the sample chamber and high-pressure regions of the carbide-tooling while increasing the efficiency of pressure generation and reducing radial stresses on the belt. In addition, the taper reduces the risk of the piston or core impinging on the neutron path in the case of minor misalignment of the cell. This simple belt profile loses some of the benefits of continuous multi-staging and large attainable compression ($\Delta V/V$) of the sample cavity that accompany more complex-curved belt designs, but is optimal for neutron access. We have currently tested the belt to sample pressures in excess of 7 GPa with no breakages.

The sample and gasket assembly are presented in figure 2. The pressure medium and inner gasket consist of CaF_2, machined from natural massive fluorite from China. These gaskets are 4.7 mm thick, measured perpendicular to the cone surface at the point of smallest diameter.

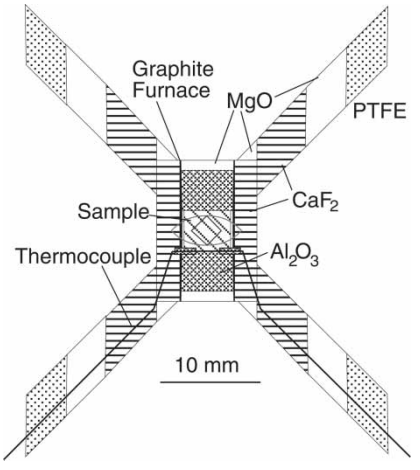

Figure 2. Schematic cross-section of the high-pressure cell.

The fluorite inner gaskets extend from 10 mm inner diameter to 25 mm outer diameter. These are surrounded by a 3 mm thick ring of semi-sintered MgO (40% porosity) and a 4 mm thick ring of PTFE, both machined such that they fill the space between the pistons and belt. The cylindrical fluorite pressure medium holds a tapered graphite furnace, sample capsule and Al_2O_3 end-plugs. Differential stress generation can be tuned by varying the relative strength and sizes of the pressure medium and end-plugs. Here we used hard polycrystalline corundum end-plugs, which generate a maximum stress down the axis of the cell of approximately twice the radial stress. The sample cavity is 3 mm long and 4 mm in diameter; in the experiments presented here, a 0.5 mm thick MgO sleeve was placed between the sample and furnace.

3. Neutron diffraction

The details of the ENGIN-X beamline are given elsewhere [4], so a description of the interaction between the new cell and the beamline will suffice here. ENGIN-X is a long-path beamline (51.5 m), with two banks of detectors at $+90 \pm 15°$ and $-90 \pm 15°$ 2θ, each covering $\pm 15°$ in ϕ. The cell is placed in the beamline such that the axis of compression is at 45° to the incident beam, which enters the cell along slot A in figure 1. The diffracted beams exiting at C sample lattice planes are perpendicular to the compression axis; upon compression, these atomic lattice planes experience the maximum compressive stress (σ_a). The diffracted beams exit at B sample lattice planes parallel to the compression axis; these planes experience the radial stress, which, in the axi-symmetric geometry employed here, is the minimum compressive stress (σ_r). In the current design, the slots cut out of the stress rings restrict the detectors which are reached by the diffracted beams to approximately one-fourth of the total available. Despite this, adequate diffraction patterns could be collected in 30–90 min. The maximum beam size is controlled by the geometry of the carbide belt insert and steel piston stress rings, which act as collimators. The maximum diffraction volume is shown in figure 2; this volume is $\sim 27\,mm^3$, including the entire sample and a small region of MgO and CaF_2.

A sample diffraction pattern from one of the two detector banks is presented in figure 3; the data collection time was 30 min. The diffraction pattern contains contributions from the sample, MgO, Al_2O_3 and CaF_2. It was found that the fluorite diffraction peaks showed strong

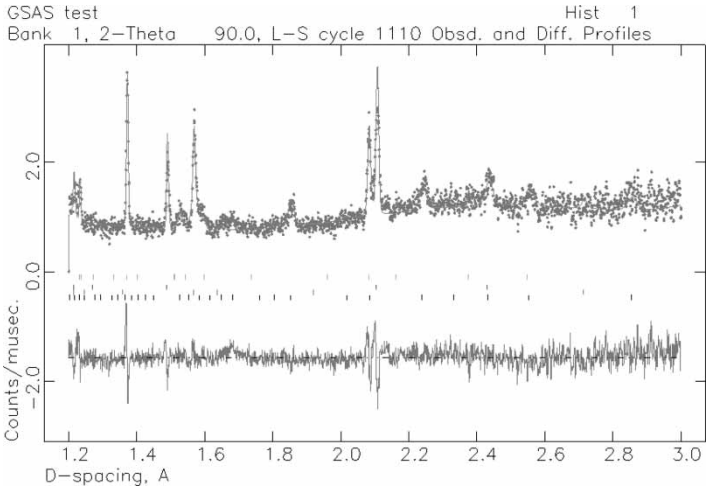

Figure 3. Sample diffraction pattern collected in 30 min at the maximum load of 23 tonnes. The upper trace is the GSGS refinement to the collected data (points) and the lower trace is the difference plot. Ticks correspond to (from top to bottom) Al_2O_3, MgO, CaF_2, $Mg_3Al_2Si_3O_{12}$.

preferential alignment because the pressure medium was cored from a coarsely crystalline natural sample; this can be avoided in future studies by pressing the pressure medium from polycrystalline CaF_2. The sample signal is small, but sufficiently clear to determine cell parameters using the known crystal structures to a precision of 10^{-4}. Diffraction patterns were fitted using the GSAS suite of programs [7]; pyrope was fitted using the Rietveld technique and the other components, which had small amounts within the diffracted volume, were fitted using the Le Bail technique. In addition to uncertainties arising from the counting statistics, there is a substantial contribution from uncertainty of sample position in the diffractometer as the pistons advance and change the sample position relative to the stationary outer frame of the press. Although the cell was optically re-centered between measurements, there was still an uncertainty of up to 0.25 mm in sample position. This equates to a variation in cell parameter of 5×10^{-5}. Future experiments will improve on this by introducing a calibrant mounted directly above the sample. Data collections from this (room P–T) calibrant can be used to determine the diffraction geometry during the experiment, as it will require only a vertical translation of the press to move from calibrant to sample.

4. Pressure calibration

The cell pressure was calibrated against oil pressure in the press using the transitions in bismuth at room temperature and at high temperature using (in order of increasing pressure) the pyrope (enstatite + sillimanite + sapphrine), albite (jadeite + quartz) and quartz (coesite) reactions. Calibrations are plotted in figure 4.

4.1 *Bi calibration*

The resistance of a thin Bi foil was monitored during slow compression and the changes associated with the Bi I–II (2.25 GPa) and III–V (7.7 GPa) transitions were observed. The radial stress was estimated using a cell in which the end-pistons were composed of fluorite. In this case, the internal strength of all the components was approximately equal and the

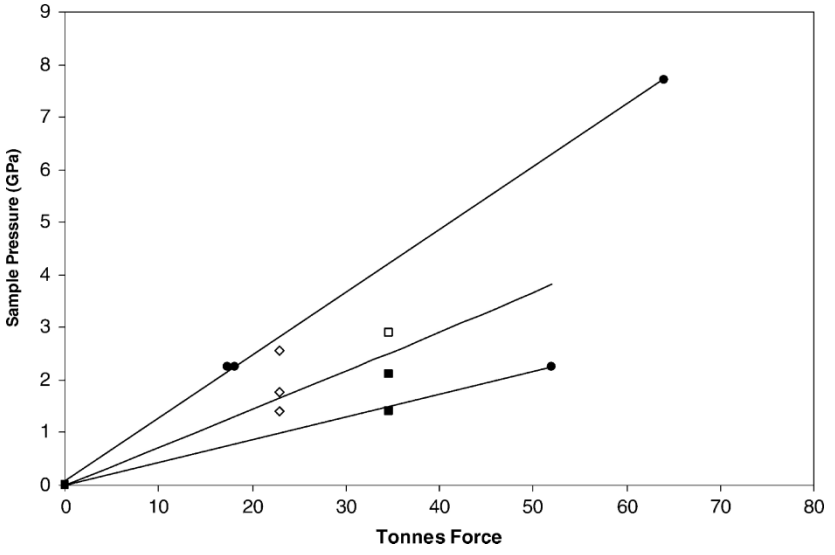

Figure 4. Sample pressure versus end-load pressure. Solid circles are for room temperature calibration points for the Bi I–II (2.25 GPa) and III–V (7.7) transition for cells with and without corundum stress guides. The solid curves are estimates of maximum, minimum and mean stress based on the Bi calibrations. Squares are for 1073 K calibrations using the pyrope (enstatite + sillimanite + sapphrine, 1.2 GPa), albite (jadeite + quartz, 2 GPa) and quartz (coesite, 3 GPa) reactions. Filled symbols denote high-pressure phase recovered and open symbols denote low-pressure phase recovered. Open diamonds are for neutron measurement of maximum, minimum and mean stress. The estimations of stress from the room temperature and quenching experiments are in good agreement with the values measured by neutron diffraction.

differential stress supported by the relatively weak fluorite is small. This is, however, likely to be a slight underestimate of the radial stress generated with the hard pistons present, as the overall compressibility of the cell assembly is higher when the corundum pistons are replaced by fluorite. This 'radial' pressure calibration curve is the lower line plotted in figure 4.

In addition to this calibration, the stress was calibrated using a cell with corundum pistons. The Bi sample was sandwiched between thin (1.5 mm) layers of semi-sintered MgO to remove any stress heterogeneities related to surface imperfections on the corundum pistons. After compression, this MgO layer was 2 mm thick, which is sufficiently thin for there to be little extrusion of MgO into the surrounding fluorite pressure medium. This calibration curve is the upper line plotted on figure 4.

4.2 *High-temperature calibration*

A high-temperature calibration experiment was performed at 1073 K and 35 tonnes end-load. The sample cavity contained three separate Pt capsules, surrounded by semi-sintered MgO. These capsules each contained one of the calibration compositions. The quartz–coesite starting material was quartz powder, whereas the other two calibrants used glass starting materials of pyrope and albite stoichiometry. The high-temperature calibration used corundum pistons and pressure and temperature were maintained for 2 h. A tungsten–rhenium thermocouple was used to measure the temperature, with the hot junction terminating on the end of the capsules. High-temperature calibrations are plotted as squares on figure 4. The high-pressure phases pyrope and jadeite + quartz were detected in recovered samples by X-ray diffraction, whereas no coesite was detected in the quartz sample. The pressure was therefore 2.5 ± 0.5 GPa. The middle solid line in figure 4 is the mean of the two Bi calibration curves (σ_m), calculated

assuming that the calibration using corundum represents the axial stress and the calibration using fluorite pistons represents the radial stress:

$$\sigma_{\mathrm{m}} = \frac{\sigma_{\mathrm{a}} + 2\sigma_{\mathrm{r}}}{3} \tag{1}$$

The mean stress, calculated in this manner, is consistent with the high-temperature calibrations. In addition, the stresses, σ_{a}, σ_{r} and σ_{m} measured by neutron diffraction (see below) at 23 tonnes load and 873 K are plotted as open diamonds in figure 4. All pressure calibrations are consistent.

5. Rheological testing

5.1 *Measurement of strain*

The high-strain resolution of the neutron diffraction technique makes it ideal for determining rheological properties at low strain rates ($\dot{\varepsilon}$) and differential stresses ($\sigma_{\mathrm{d}} = \sigma_{\mathrm{a}} - \sigma_{\mathrm{r}}$). The belt-type design developed here does not have independent strain control and pressure control, so the stress relaxation technique must be employed [8, 9]. The sample is loaded to some differential stress and allowed to deform. There is an instantaneous elastic deformation of the sample:

$$^{\mathrm{e}}\varepsilon_i = s_{ij}\sigma_j, \tag{2}$$

where s_{ij} are the elastic compliances of the sample and $^{\mathrm{e}}\varepsilon_i$ are the elastic strain resulting from the applied stress, σ_j. At high temperature, however, the sample starts to deform plastically:

$$^{\mathrm{t}}\varepsilon = {}^{\mathrm{e}}\varepsilon + {}^{\mathrm{p}}\varepsilon. \tag{3}$$

If the load cell is sufficiently stiff, that is, if its deformation is negligible, the total strain ($^{\mathrm{t}}\varepsilon$) in the sample remains constant and the plastic strain ($^{\mathrm{p}}\varepsilon$) can be determined by monitoring the change in elastic strain with time. The press can be made to imitate a stiff system by ensuring that the displacement of the pistons used to load the sample remains constant. This is achieved by careful feedback control, *i.e.* adjusting the oil pressure in the ram to maintain a constant displacement between the carbide pistons. In this case, only the sample strain and elastic strain in the pistons contribute to the total strain. The pistons are short and very hard, consisting of tungsten carbide and produce a negligible contribution to the observed sample rheology (the maximum load used here will produce only 0.5 μm of elastic strain in the pistons). With a solid medium apparatus, there is, however, an additional complication of plastic deformation of the gaskets and pressure medium. Gasket flow in the current arrangement results in an increase in the axial stress and a drop in the radial stress. It is generally found, for a range of solid-media devices, that upon initial heating the gaskets flow plastically until some critical threshold of gasket thickness is reached, at which time the plastic flow ceases. Subsequent heating causes an increase in the sample pressure because of the thermal expansion of the sample and cell. The change in stresses with temperature, at constant end-load, are plotted in figure 5. It can be seen that between 673 and 873 K there is a significant increase in pressure and that the increase in both the axial and radial stresses are approximately equal. The gaskets have therefore stopped flowing by this temperature and the pressure change is due to the thermal pressure of the cell and sample. The current gasket design is therefore appropriate to rheological testing at temperatures of 873 K and above.

In addition to the redistribution of stress by gasket flow, the observed rheology contains a contribution from the flow of the pressure medium around the sample as the sample deforms.

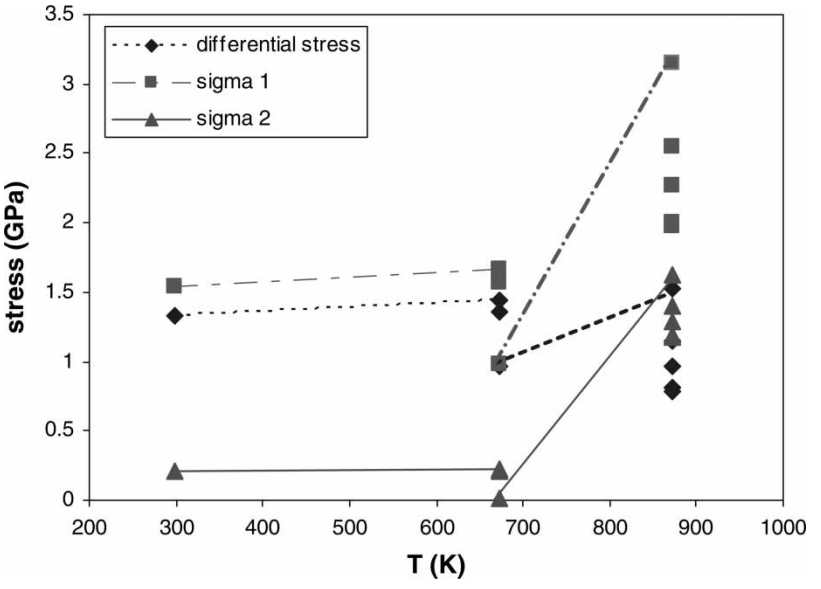

Figure 5. Stress versus temperature at 23 tonnes end-load. Between 298 and 673 K the increase in thermal pressure is offset by cell relaxation but between 673 and 873 K there is little relaxation and the increase in thermal pressure is evident. The data points at constant temperature are the annealing steps at 673 and 873 K.

The use of a pressure medium which is significantly softer than the sample ensures that its contribution does not materially affect the observed rheology of the sample.

5.2 *Measurement of stress*

For an axi-symmetric experimental system, with a sample which consists of an isotropic average of grains of cubic symmetry, the bulk axial and radial strains are given by [10]:

$$^{\mathrm{e}}\varepsilon_{\mathrm{a}} = s_{11}\sigma_{\mathrm{a}} + 2s_{12}\sigma_{\mathrm{r}} \tag{4}$$

$$^{\mathrm{e}}\varepsilon_{\mathrm{r}} = s_{11}\sigma_{\mathrm{r}} + s_{12}(\sigma_{\mathrm{a}} + \sigma_{\mathrm{r}}) \tag{5}$$

and the stresses by:

$$\sigma_{\mathrm{a}} = \left(\frac{(s_{11} + s_{12})^{\mathrm{e}}\varepsilon_{\mathrm{a}} - 2s_{12}{}^{\mathrm{e}}\varepsilon_{\mathrm{r}}}{(s_{11} - s_{12})(s_{11} + s_{12})}\right) = c_{11}{}^{\mathrm{e}}\varepsilon_{\mathrm{a}} + 2c_{12}{}^{\mathrm{e}}\varepsilon_{\mathrm{r}} \tag{6}$$

and

$$\sigma_{\mathrm{r}} = \left(\frac{s_{11}{}^{\mathrm{e}}\varepsilon_{\mathrm{r}} - s_{12}{}^{\mathrm{e}}\varepsilon_{\mathrm{a}}}{(s_{11} - s_{12})(s_{11} + s_{12})}\right) = c_{11}{}^{\mathrm{e}}\varepsilon_{\mathrm{r}} + c_{12}({}^{\mathrm{e}}\varepsilon_{\mathrm{r}} + {}^{\mathrm{e}}\varepsilon_{\mathrm{a}}) \tag{7}$$

where σ_{a}, σ_{r}, $^{\mathrm{e}}\varepsilon_{\mathrm{a}}$ and $^{\mathrm{e}}\varepsilon_{\mathrm{r}}$ are the axial and radial stresses and elastic strains and s_{11}, s_{12}, c_{11} and c_{12} are the compliances and stiffnesses of the isotropic aggregate.

Neutron diffraction measures the separation of lattice planes and hence the elastic strains associated with each plane; in general, these strains will not be simply related to the applied bulk stresses. Even cubic crystals do not behave isotropically under uniaxial loading [10]; for

such crystals, a single-crystal plane-specific modulus, $E_{h\,k\,l}$, may be written as [11]:

$$\frac{1}{E_{h\,k\,l}} = s_{11} - 2\left(s_{11} - s_{12} - \frac{1}{2}s_{44}\right)\left[\frac{h^2k^2 + h^2l^2 + k^2l^2}{\left(h^2 + k^2 + l^2\right)^2}\right] \tag{8}$$

where the term in brackets has limiting values of 0 for $h\,0\,0$ reflections and 1/3 for $h\,h\,h$ reflections. This equation, however, assumes a 'free' single crystal, whereas, in reality, each grain in an aggregate will exhibit elastic properties somewhere between the Reuss bound (uniform stress) and the Voigt bound (uniform strain) [12, 13]. Refs. [11] and [14] give examples of the ways in which these problems may be addressed, for example, by including an $h\,k\,l$-dependent peak shift into a Rietveld refinement program. In the present pilot experiment, the relatively poor quality of the data prohibits the use of such an approach. We have, instead, simply derived mean values of ${}^{\mathrm{e}}\varepsilon_{\mathrm{a}}$ and ${}^{\mathrm{e}}\varepsilon_{\mathrm{r}}$ from the 'Rietveld strains', *i.e.* from the lattice parameter values determined by standard Rietveld refinement (assuming cubic symmetry) of the data from each of the two detector banks, which sample, respectively, lattice planes aligned perpendicular to and parallel to the axis of the cell.

In order to infer the stresses corresponding to the strains, ${}^{\mathrm{e}}\varepsilon_{\mathrm{a}}$ and ${}^{\mathrm{e}}\varepsilon_{\mathrm{r}}$, values of the elastic constants are required. Garnets provide a favourable case for studies such as that reported here as they are often very close to being elastically isotropic (*i.e.* $s_{44} = 2(s_{11} - s_{12})$) and thus the required moduli for the polycrystalline aggregate calculated in the Voigt and Reuss approximations are almost identical to each other and to those for the free single crystal [15]; the differences between measurements for pyrope reported by different workers are far larger. A more serious problem arises from the lack of published data on the pressure and temperature dependence of individual elastic moduli, $\mathrm{d}c_{ij}/\mathrm{d}P$ and $\mathrm{d}c_{ij}/\mathrm{d}T$; in general, only quantities such as the pressure-dependence of bulk moduli ($K' = \mathrm{d}K/\mathrm{d}P$) are readily available. A possible solution to this problem in future work would be to combine the values of c_{ij} measured under ambient conditions with first-principles computer simulation of their pressure and temperature dependence [16]. In the present pilot study we have considered it sufficient to use the single-crystal values of $c_{11} = 296.2$ GPa and $c_{12} = 111.1$ GPa measured under ambient conditions [17], as to some extent the increase in stiffness produced by the elevated pressure will be offset by softening at high temperature.

6. Sample data: strength of Dora Maira pyrope at 873 K

Figure 6 shows the evolution with time of elastic strain in the axial direction for stress relaxation at 673 and 873 K. At each temperature equation (3) holds (thermal pressure induces extra strain on heating) and the plastic strain curve is the complement of the elastic strain curve. The solid curves are power-law fits of strain against time. At 873 K the strain rate drops to 1.7×10^{-8}/s after 6 h. This low strain rate results in a strain change of 10^{-4} per data collection at the current collection rate of 30–90 min per collection. A strain change of 10^{-4} is approximately five times smaller than the formal error (1σ) on the fit to the diffraction data. However, the scatter in the data is considerably better than this, suggesting that strain rates can be measured down to 10^{-8}/s, or better, in a relatively short (<24 h) experiment. The main source of imprecision in peak-fitting in the current experiment is due to the strong peak-broadening in the non-isotropic pressure environment. At higher temperatures, or after longer annealing durations, the precision should significantly improve.

The variation of differential stress with time, derived from the measured strains via equations (6) and (7), is plotted in figure 7. Once again, the formal error is significantly larger than

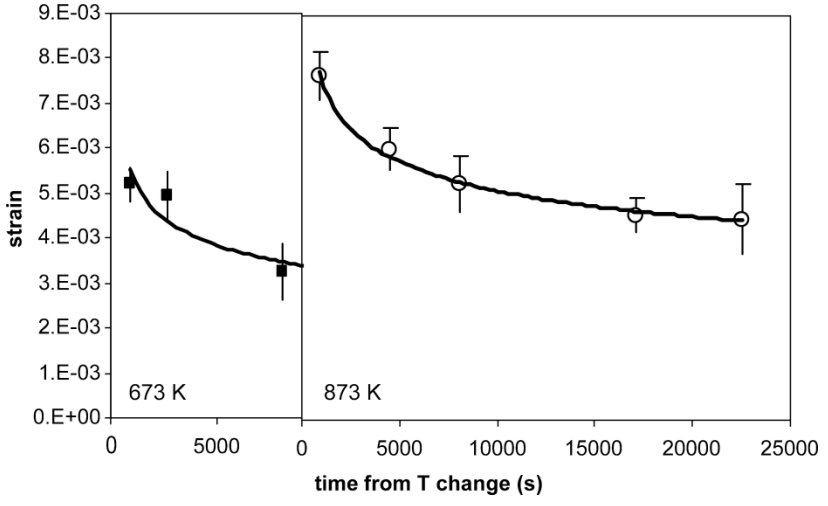

Figure 6. Axial elastic strain versus time from temperature change for Dora Maira pyrope at 673 and 873 K. The mean stress is 0.5 GPa at 673 K and 1.75 GPa at 873 K. Solid curves are power-law fits to the data.

the apparent scatter in the data. Isothermal stress relaxation at 673 and 873 K is clear, as is the increase in stress on heating, owing to thermal pressure.

Deformation within the dislocation climb regime obeys a power law relationship with strain rate dependent on some power of the stress:

$$^{\mathrm{p}}\dot{\varepsilon} = A_0 \exp\left(\frac{-Q}{RT}\right)\sigma^n \tag{9}$$

where Q is the activation energy of creep, and R and T have the usual meanings. Equation (9) can be linearised by taking logarithms of the strain rate and stress, as shown in figure 8. The strain rate was determined from the fit to data shown in figure 6. We find A_0 and n to be $4.6 \pm 0.4 \times 10^{-7}$ and 5.5 ± 0.3, respectively; $R^2 = 0.990$ at 873 K. The stress exponent is

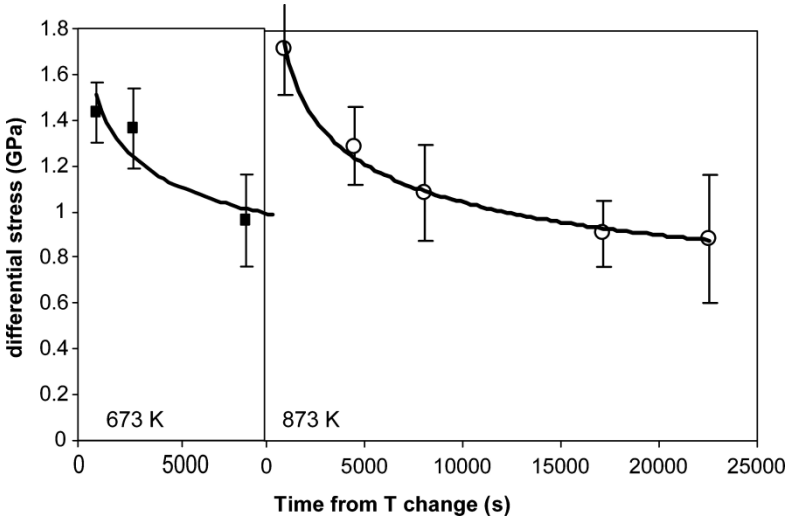

Figure 7. Differential stress versus time from temperature change for Dora Maira pyrope at 673 and 873 K. The mean stress is 0.5 GPa at 673 K and 1.75 GPa at 873 K. Solid curves are power-law fits to the data.

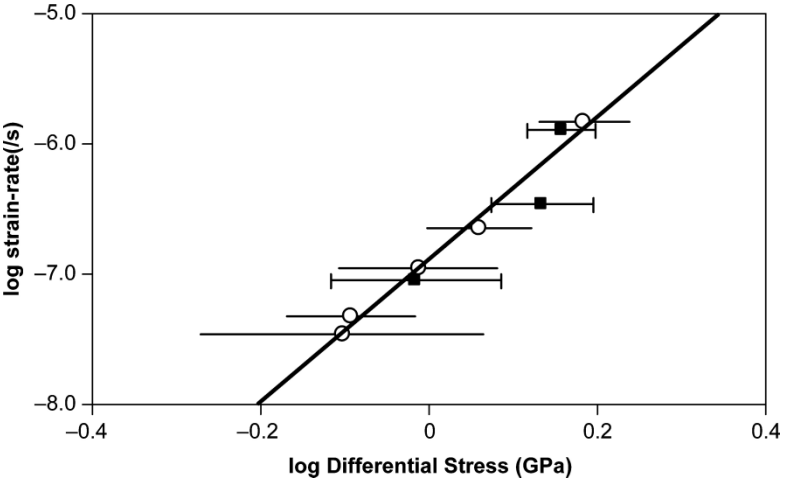

Figure 8. log (strain rate) versus log (differential stress): a power-law fit. Open circles at 873 K and solid squares at 673 K. The power-law fit to the 873 K data gives $\dot{\varepsilon} = 4.6(4) \times 10^{-7}\sigma^{5.5(3)}$ (errors in the last digit in parentheses).

somewhat larger than that found in a previous study [18] which found an n of 3.2 ± 0.7 for experiments in the temperature range 1073–1573 K and pressures of 5–6 GPa.

The present experiments are likely to be below the temperature where climb-assisted dislocation glide becomes dominant [5, 19] and within the low-temperature glide field, with a strain rate dependence on stress of:

$$^{\mathrm{p}}\dot{\varepsilon} \propto \left(\frac{\sigma}{\mu}\right)^2 \exp\left(\frac{-Q + \beta\sigma}{RT}\right) \tag{10}$$

where μ is the shear modulus and β is a constant. The exponential stress term dominates in equation (10) and plots of stress versus log (strain rate) for deformation in the glide field are approximately linear (figure 9). Equations (9) and (10) fit the 873 data equally well, with $((Q + \beta\sigma)/RT) = 6.2 \pm 0.3$ and $(\sigma/\mu)^2 = 8.2 \pm 1.7 \times 10^{-10}$; $R^2 = 0.994$, however

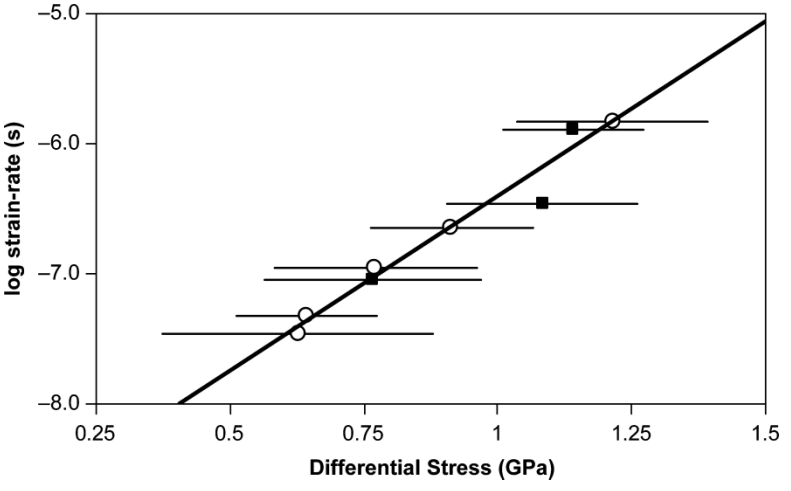

Figure 9. log (strain rate) versus differential stress: an exponential fit. Open circles at 873 K, solid squares at 673 K. The exponential fit to the 873 K data gives $\dot{\varepsilon} = 8.2(1.7) \times 10^{-10}\mathrm{e}^{6.2(3)\sigma}$ (errors in the last digit in parentheses).

the similarity of the stress dependence at 673 and 873 K suggests that the current experiments are in the glide field with a weak temperature dependence. The observed strain rate at 873 K and 0.5 GPa differential stress is two orders of magnitude higher than the value extrapolated from Li *et al.* [18] to the same conditions, consistent with a change in mechanism between 1073 and 873 K.

7. Summary and conclusion

The new belt-type device presented here provides a high-pressure environment for strain measurements using the ENGIN-X neutron diffractometer at pressures up to at least 7 GPa. Data collections of 60 min, or shorter, allow time series to be collected for stress relaxation experiments. The counting rate can be further improved by minor modifications (currently under construction) to the cell and piston design and we expect in the future to be able to use the entire detector bank on ENGIN-X, increasing the data rate by a factor of four. The high-strain resolution possible on ENGIN-X allows strain rates of 10^{-9}/s, or lower, to be readily determined by the use of interrupted testing. Attaining very low strain rates is important for extrapolations to geological conditions; the device presented here currently provides the lowest attainable strain rates of the high-pressure rheological devices.

References

[1] D.J. Weidner, Y. Wang, G. Chen *et al.*, in *Properties of Earth and Planetary Materials at High Pressure and Temperature*, Geophysics Monographs volume 101, p. 473, edited by M. Manghnani and Y. Yagi (American Geophysical Society, Washington DC, 1998).
[2] Y.B. Wang, W.B. Durham and I.C. Getting, Rev. Sci. Instrum. **74** 3002 (2003).
[3] W.B. Durham, D.J. Weidner, S.I. Karato *et al.*, Rev. Mineral. Geochem. **51** 21 (2002).
[4] M.W. Johnson and M.R. Daymond, J. Appl. Cryst. **35** 49 (2002).
[5] Z.C. Wang and S.C. Ji, Can. Mineral. **37** 525 (1999).
[6] J.M. Besson, R.J. Nelmes, G. Hamel *et al.*, Physica B **180 and 181** 907 (1992).
[7] A.C. Larson and R.B. Von Dreele, Los Alamos Laboratory Report LA-UR-86-748 (1986).
[8] E.H. Rutter, B.K. Atkinson and D.H. Mainprice, Geophys. J. Roy. Astro. Soc. **55** 155 (1978).
[9] S.J. Covey-Crump, J. Geophys. Res. **103** 29781 (1998).
[10] J.F. Nye, *Physical Properties of Crystals: Their Representation by Tensors and Matrices* (Oxford University Press, 1985).
[11] M.R. Daymond, M.A.M. Bourke, R.B. Von Dreele *et al.*, J. Appl. Phys. **82** 1554 (1997).
[12] J.P. Poirier, *Introduction to the Physics of the Earth's Interior* (Cambridge University Press, Cambridge, 1991).
[13] J.M.J. den Toonder, J.A.W. van Dommelen and F.P.T. Baaijens, Model Simul. Mater. Sci. **7** 909 (1999).
[14] M.R. Daymond, J. Appl. Phys. **96** 4263 (2004).
[15] G. Simmonds and H. Wang, *Single Crystal Elastic Constants and Calculated Aggregate Properties: A Handbook*, 2nd edn (M.I.T. Press, Cambridge MA, 1971).
[16] L. Vocadlo, D. Alfe, M.J. Gillan *et al.*, Phys. Earth Planet. Sci. **140** 101 (2003).
[17] B. O'Neill, J.D. Bass, G.R. Rossman *et al.*, Phys. Chem. Mineral. **17** 617 (1991).
[18] L. Li, P. Raterron and D. Weidner, submitted to American Mineralogist.
[19] V. Voegele, J.I. Ando, P. Cordier *et al.*, Phys. Earth Planet. Int. **108** 305 (1998).